RESEARCH ARTICLE

Role of Exosomes from Nucleus Pulposus Cells in Attenuating Intervertebral Disc Degeneration by Inhibiting Nucleus Pulposus Cell Apoptosis via the miR-8485/GSK-3 β /Wnt/ β -catenin Signaling Axis

Weiye Zhang^{1,#}, Ping Zhang^{1,#}, Jiawen Zhan^{1,*}, Xu Wei¹, Yuxuan Du¹, Ke Zhao¹, Liguo Zhu¹, Rong Xie¹, Hualong Xie¹, Shuaiqi Zhou¹, Gewen Wang¹ and Chuhao Cai¹

¹China Academy of Chinese Medical Sciences Wangjing Hospital, No. 6 Zhonghuan South Road, Chaoyang District, Beijing, China

© 2025 The Author(s). Published by Bentham Science Publisher. This is an open access article published under CC BY 4.0 https://creativecommons.org/licenses/by/4.0/legalcode

Abstract: *Background*: Studies have shown that abnormal stress is a significant inducer of Intervertebral Disc Degeneration (IVDD). Although traction force is commonly used to delay IVDD, its effects on Nucleus Pulposus Cells (NPCs) and their secreted exosomes remain unclear. In addition, this study systematically revealed the relationship between miR-8485 and IVDD for the first time.

Methods: Cellular experiments were performed using a Flexcell cell stretching platform to apply traction force to NPCs. After optimizing loading parameters, NPC-derived exosomes (NPCs-exo) were isolated and subjected to miRNA high-throughput sequencing. Differentially expressed miRNAs were identified, and their regulatory effects on the Wnt/β-catenin pathway were investigated. *Ex vivo* rabbit spinal samples were used to validate the cellular experimental results under traction force loading.

Results: NPCs-exo were found to be internalized by NPCs, and traction force promoted NPCs-exo secretion. High-throughput sequencing and differential expression analysis identified miR-8485 as a differentially expressed miRNA in NPCs-exo secreted under Cyclic Mechanical Tension (CMT) conditions. Dual-luciferase reporter assays confirmed the targeted regulatory relationship between miR-8485 and GSK-3β, as well as its involvement in the Wnt/β-catenin pathway-mediated regulation of NPCs degeneration. *Ex vivo* experiments, including morphological and immunofluorescence analyses, revealed that the traction group exhibited better morphology than the pressure group, with a more organized AF, NP, and higher NPCs content, though some loss persisted. Both groups showed significant differences in ECM markers (Collagen II, Aggrecan, MMP3) compared to the control (p < 0.05). Additionally, the traction group had significantly higher Collagen II and Aggrecan levels than the pressure group (p < 0.05).

Conclusion: CMT can promote the secretion of NPCs-exo, which are internalized by the NPCs. Through the delivery of miR-8485, NPCs-exo target and regulate GSK-3β, thereby enhancing Wnt/β-catenin pathway activity. This mechanism increases NPCs viability and extracellular matrix synthesis while suppressing apoptosis, ultimately delaying IVDD progression. Immunofluorescence staining in animal experiments confirmed that traction force effectively improves extracellular matrix expression in the IVD and mitigates stress-induced morphological alterations of the IVD.

Keywords: Nucleus pulposus cells, exosomes, intervertebral disc degeneration, traction force, miR-8485.

1. INTRODUCTION

ARTICLE HISTORY

10.2174/0115665240370788250617070218

Received: December 03, 2024

Revised: February 27, 2025

Accepted: March 04, 2025

The Intervertebral Disc (IVD) is a crucial structure for bearing the body's load, with its development

ny of thuan t

beginning in the third week of embryogenesis [1, 2]. It functions to absorb shock, distribute external forces, and maintain spinal stability [3, 4]. The Nucleus Pulposus (NP) is a gel-like avascular tissue located in the central region of the IVD. It is primarily composed of type II collagen, with small amounts of other collagen types and proteoglycans. Its main function is to distribute the body's load in various directions within each IVD under compressive forces [5]. As an

^{*}Address correspondence to this author at the China Academy of Chinese Medical Sciences Wangjing Hospital, No. 6 Zhonghuan South Road, Chaoyang District, Beijing, China;

E-mails: zhangweiyexs@outlook.com; zhanjiawen12@126.com

^{*}These authors contributed equally to this work.

avascular tissue, the NP relies on nutrient supply primarily through passive diffusion from the highly vascularized vertebral endplates via the Cartilaginous Endplate (CEP) located above and below it [6, 7].

Research indicates that abnormal stress is a significant inducer of Intervertebral Disc Degeneration (IVDD). A histological study on age-related changes in human IVDs demonstrated that reduced blood supply to the Cartilaginous Endplate (CEP) is a crucial factor leading to Nucleus Pulposus (NP) rupture during the second decade of life [8]. Our previous research also indicated that abnormal stress-induced degeneration of the CEP, which results in impaired nutrient metabolism and substance transport, plays a vital role in the onset and progression of IVDD [9]. Nucleus Pulposus Cells (NPCs), the primary cell type in NP tissue, are regulated by various factors within the complex microenvironment of the IVD [10, 11]. However, the detailed mechanisms underlying NPCs' changes and under abnormal degeneration stress insufficiently understood. Investigating the effects of abnormal stress on the NPC microenvironment within the IVD can help elucidate the mechanisms of stressinduced IVD degeneration, laying a foundation for the prevention, treatment, and early repair of IVDD. Exosomes (EXO) are considered crucial mediators in local microenvironment regulation [12], and engineered EXO can deliver relevant drugs and small molecules to alleviate IVDD [13]. Studies have shown that human NPCs can secrete EXO, which can influence IVDD [14], and stress can regulate the secretion process of NPCs-exo, affecting the stability of the IVD microenvironment [15]. Current research suggests that EXO can influence IVDD by delivering miRNA. These miRNAs may play a pivotal role in modulating cellular processes within the disc, potentially offering a therapeutic avenue for mitigating the degenerative changes associated with IVDD [16-19].

As a form of abnormal stress, Cyclic Mechanical Tension (CMT) is involved in regulating the complex biological processes and signalling pathways of IVD [20]. However, its potential role in delaying IVDD progression remains unknown. Recent studies have shown that the activity and apoptosis of NPCs can be influenced by EXO from other cell sources [21], but the effects of NPCs-exo on NPCs under CMT conditions remain unclear. Following CMT loading, miR-8485 exhibited significant differential expression in NPCsexo. Previous research indicates that miR-8485 can modulate the Wnt/β-catenin pathway, influencing chondrocyte function and arthritis progression. However, its potential involvement in IVDD regulation has not been investigated, leading to the initiation of this study. Therefore, this study aims to observe the changes in NPCs-exo under CMT stimulation and the effects of NPCs-exo on NPCs under co-culture conditions. By exploring the changes and interactions of NPCs and their autocrine EXO under CMT conditions, an ex vivo spinal unit loading and culture device (ESLCD) [22] was used to apply tensile loading to animal ex vivo spinal motion segments and observe the effects of tensile loading on the intervertebral discs

and nucleus pulposus of animal spinal motion segments. Additionally, an animal IVDD model was prepared, and the effect of NPCs-exo injection on delaying IVDD in animals was observed.

Table 1. Experimental grouping for CMT parameter screening.

Group	Traction Rate	Frequency	Duration
Step 1	-	-	-
Control	0	0	24 hours
Blank	0	0	24 hours
А	5%	1Hz	24 hours
В	10%	1Hz	24 hours
Step 2	-	-	-
Control	0	0	24 hours
Α	X	0.5Hz	24 hours
В	X	1Hz	24 hours
С	X	5Hz	24 hours

2. MATERIALS AND METHODS

2.1. Cell Experiments

NPCs were isolated from traumatic lumbar disc surgeries performed at our hospital. Patients from whom NPCs were isolated underwent detailed examination and screening, following the methods outlined by Wan et al [23]. The degenerative condition of the IVD was assessed using Magnetic Resonance Imaging (MRI) according to the Pfirrmann grading system [24]. The inclusion criteria were as follows: 18 < age < 30, Pfirrmann grade = 1, and the NPCs were harvested from the L3-L5 intervertebral disc region. Informed consent was obtained from the patients, and the study protocol strictly adhered to the ethical requirements and was approved under the approval number WJEC-KT-2020-014-P001.

2.1.1. Isolation and In Vitro Culture of NPCs

Referring to published studies and methodologies [25], the excised NP tissue was meticulously cleared of any attached endplate and annulus fibrosus tissue under sterile conditions. The NP tissue was then finely minced with tissue scissors, washed in PBS, and transferred to centrifuge tubes containing type II collagenase to ensure thorough immersion in the solution. The tissue was digested at 37°C for 12 hours. The cell suspension was collected, and an equal volume of complete medium (10% fetal bovine serum + 100 U/mL penicillin-streptomycin + DMEM/F-12 medium) (Gibco, USA) was added. The mixture was centrifuged at 1200 r/minute for 6.5 minutes, and then 5 mL of complete medium was added to resuspend the cells. The cells were then seeded into 25 cm2 vented culture flasks and cultured at 37°C, 5% CO2, and 95% humidity. The culture medium was replaced every three days, and cell growth was monitored under a micro-

scope. When NPCs reached 80%-90% confluency, they were plated onto Flexcell tension plates.

2.1.2. CMT Loading of NPCs

The NPCs were seeded onto Flexcell tension plates at 50% confluency and incubated overnight at 37°C to allow for cell adhesion. Before applying CMT, the medium in the Flexcell tension cell culture plates (FTCCP) was replaced with 2 mL of corresponding serum-free medium to avoid interference from EXO present in the serum during subsequent NPCs-exo extraction. To determine the CMT parameters that have minimal impact on NPCs' activity, the strain rate and frequency parameters were screened in two steps. The frequency was set to 1 Hz. The strain rate parameter in Step 2, denoted as X, was determined based on the screening results from Step 1. The determination of the strain rate depends on NPCs' cell viability, as assessed by the CCK-8 assay, to select the optimal strain rate parameter. To eliminate any potential impact of the Flexcell tension plates on cell activity, a control group was established (Table 1).

2.1.3. Measurement of Proliferation Activity of **NPCs**

After digestion with trypsin, NPCs loaded with CMT were seeded at 5×10³ cells per well in sterile 96-well cell culture plates and incubated for 12 hours. Subsequently, each well was supplemented with serum-free DMEM medium containing 10 µL of CCK-8 reagent, followed by further incubation at 37°C in the dark for 2 hours. Absorbance was measured at 450 nm using a microplate reader.

2.1.4. Isolation of NPCs-exo

Using the EXO Extraction Kit (China Meilun Biotech), NPCs-exo were separated and purified using magnetic bead-based isolation. Supernatants of NPCs cultures post-loading were collected using a pipette, 550 µL of which were transferred to a new 1.5 mL centrifuge tube and centrifuged at 4°C, 3000 grams for 10 minutes. The resulting 500 µL supernatant was then transferred to a new 1.5 mL centrifuge tube for further processing. Following the protocol of the EXO Extraction Kit, NPCs-exo were separated into CMT-NPCs-exo and NPCs-exo groups in the centrifuge tubes containing pre-treated samples.

2.1.5. Characterization and Identification of NPCsexo

50 µL of NPCs-exo suspension was dropped onto a copper grid, allowed to stand at room temperature for 1 minute, and the excess liquid was removed from the side using filter paper. Approximately 20 µL of 2% phosphotungstic acid solution (pH 6.8) was applied to the grid and stained negatively for 1 minute at room temperature. The excess stain was blotted with filter paper, and the grid was allowed to air dry. Furthermore, it was observed and photographed under a transmission electron microscope (HT7830, Hitachi, Tokyo, Japan). All protein expression levels were determined via Western blot analysis. The total protein of cells and exosomes was extracted using the BCA

protein extraction kit (Beyotime Biotechnology, China). The protein samples were added to the loading buffer and boiled for 5 minutes. Following the treatment, the proteins were separated using sodium dodecyl sulfatepolyacrylamide (SDS) gels (12%) by polyacrylamide gel electrophoresis (PAGE, Beyotime Biotechnology, China). The proteins were transferred to polyvinylidene fluoride membranes (PVDF membranes, Millipore, United States) using a wet blotting method. Following blocking with 5% non-fat milk in Tris-buffered saline containing 0.1% Tween-20 (TBST) for 1 hour, the membranes were incubated overnight at 4°C with suitable primary antibodies. After being washed 3 times in TBST, the membranes were incubated with the secondary antibodies for 2 hours at room temperature. After adding ECL luminescence solution, the bands were detected using the Li-Cor Odyssey 9120 Infrared Imaging System (Bio-Rad, United States). The intensity of bands was quantified through the ImagePro Plus software (Version 6.0, Media Cybernetics, United States). The antibodies used are as follows: Calnexin (1:1,000, Abcam, United Kingdom), CD63 (1:1,000, Abcam, United Kingdom), and TSG101 (1:1,000, Abcam, United Kingdom). The antibody for GAPDH (1:2000; Abcam, United Kingdom) was used as a control.

2.1.6. Flow Cytometry Detection

200 µL of the homogenized NPCs-exo suspension was taken per tube after separation and purification. 0.2 µL of CFSE staining reagent (Solarbio) was added to each tube, which were then incubated at 37°C in the dark for 10 minutes, followed by detection using a flow cytometer. The CMT group, the No-CMT group, and the blank group were set up. For the blank group, neither dye nor the test sample was added. Flow cytometric detection was then performed.

2.1.7. NPCs-exo Size Detection

The diluted NPCs-exo solution was introduced into a Nanoparticle Tracking Analysis (NTA) instrument to detect the size of the exosomes. The working principle of NTA involves collecting the scattered light signals from the particles, observing the Brownian motion of the exosomes in the solution, and performing tracking and analysis.

2.1.8. PKH67 Fluorescent Labelling of NPCs-exo

NPCs-exo were labelled according to the instructions of the PKH67 fluorescent dye kit (Fluorescence). Specifically, the PKH67 reagent was allowed to reach room temperature, then diluted 10-fold with the diluent provided. Next, the PKH67 stock solution was diluted 25-fold with PBS to prepare the staining working solution. The prepared NPCs-exo were resuspended in 100 µL of the staining working solution and incubated at 37°C for 5 minutes, followed by incubation at 4°C for 15 minutes. After staining, 400 μL of PBS was added.

2.1.9. Observation of NPCs Uptake of NPCs-exo

NPCs were cultured following method 3.1. When the cell density reached 80%, the cells were passaged at a 1:3 ratio. PKH67-labelled and purified NPCs-exo were used. 500 μ L of NPCs-exo was added to NPCs at 30% cell density and co-cultured for 24 hours. The following experimental groups were set up, following dissociation of the cells with trypsin into a single cell suspension using the culture medium. The cell suspension was smeared directly onto slides, and fluorescence imaging was performed under an inverted fluorescence microscope. The NPCs co-cultured in each group were analyzed for apoptosis rate and cell proliferation activity using a flow cytometer.

2.1.10. qPCR Detection

Total RNA was extracted using the TRIzol method (Takara, Japan) according to the manufacturer's instructions. cDNA synthesis was performed using a reverse transcription kit (Promega, USA). The reaction mixture was then placed in a quantitative real-time PCR (qPCR) instrument. PCR cycling conditions were set as follows: initial denaturation at 95°C for 10 minutes, followed by 45 cycles of denaturation at 95°C for 15 seconds, and annealing/extension at 60°C for 1 minute. qPCR primer sequences were synthesized by Shanghai Sangon Biotech Co., Ltd. Untreated NPCs served as both the blank control and positive control groups. GAPDH was used as the internal reference gene. The relative mRNA expression levels of Aggrecan, Collagen II, and MMP3 in NPCs from each experimental group were calculated using the 2\(^{-}\) $\Delta\Delta$ Ct) method (Table **2**).

2.1.11. High-throughput Sequencing and Analysis of NPCs-exo miRNA

Total RNA was isolated from NPCs-exo using the Total EVs RNA Isolation Kit (RiboBio, China). RiboBio assessed the quality and quantity of the miRNA and constructed and sequenced the miRNA library. The library was sequenced using the HiSeq 2500 system (Illumina, USA), and the Illumina analysis software was applied to the raw read data. Data normalization: The miRNA sequencing data were normalized using the "limma" package in R language. Differential expression analysis: The DESeq2 software was used for differential analysis of miRNA between the two groups, with screening criteria of |log2(Foldchange)| > 1 and p < 0.05. Potential target genes of the differentially expressed miRNAs were predicted using databases such as TargetScan, miRDB, miRbase, miRTarBase, miRWalk, and miRPathDB. Gene Ontology (GO) analysis was performed to identify the potential functions of the target genes. The Kyoto Encyclopedia of Genes and Genomes (KEGG) was used to predict the signalling pathways involved with the target genes.

2.1.12. Dual-luciferase Reporter Assay

Wild-Type (WT) or Mutant (MT) GSK- 3β transfection plasmids were constructed. The miRNA mimics and GSK- 3β overexpression plasmid were synthesized by iScienceX (Beijing) Co., Ltd. NPCs were seeded in a 6-well plate 24 hours before transfection. When the cells reached 40-50% confluency, the miRNA mimics were transfected according to the manufacturer's instructions using

Lipofectamine 2000 (Invitrogen, USA). The cells were harvested 48 hours after transfection for subsequent experiments.

2.2. Animal Experiments

2.2.1. Experimental Animals and Tissue Samples

All experimental procedures were conducted in accordance with the institutional guidelines for the care and use of laboratory animals at the China Academy of Chinese Medical Sciences. The experimental subjects consisted of 27 male New Zealand White rabbits, each approximately 18 weeks old and weighing around 3.0 kg. The utilization of these animals followed the protocol approved by the Animal Ethics Committee of China Academy of Chinese Medical Sciences (No: 20180406). Prior to the experiment, the rabbits were housed for one week in an environment where the temperature was maintained between 18-24°C and the relative humidity ranged from 40-70%. The facility provided adequate ventilation and a 12-hour light/12hour dark cycle. Each rabbit was caged individually to ensure ample space for movement, as well as ease of cleaning and disinfection. The rabbits were allowed access to food and water.

The animals were anesthetized with pentobarbital (100 mg/kg). Five minutes prior to euthanasia, 25,000 IU of heparin was administered via the auricular vein. Following euthanasia by CO₂ asphyxiation, the soft tissues and posterior elements of the spine were excised. In accordance with previously published sampling methods [27], a single motion segment (L4/5) was harvested from each rabbit for analysis. These segments encompassed the entire intervertebral disc, including the CEP, AF, and NP, as well as the adjacent vertebral bodies. As it was an in vitro experiment, all the rabbits were euthanized, and the spinal column samples were systematically dissected and collected, and then randomly assigned to different groups for experimentation. During the experimental process, a blind design was implemented, where the individual responsible for grouping and the one conducting the experiments were kept separate, ensuring that the experimenter remained unaware of the assignments.

2.2.2. Preparation of Ex Vivo Segment Culture Medium

Based on the established protocol [28], a culture medium suitable for the specimens was prepared. Dulbecco's Modified Eagle's Medium (DMEM) was supplemented with 50 mg/mL L-ascorbate, 100 U/mL penicillin, 100 mg/mL streptomycin, and 2.5 mg/mL Fungizone. The osmolarity of the DMEM was adjusted to 410 mOsm/kg through the addition of NaCl.

2.2.3. Ex Vivo Spinal Loading Device for Rabbit Spinal Motion Segments (ESLCD)

The ESLCD, an upgrade of a previously published design [9], features fully automated mechanical loading and culture capabilities under sterile conditions (Patent No. CN115372149B). Following thorough cleaning and

of all **ESLCD** high-temperature sterilization components, the FSUs were secured to the culture bottles of the ESLCD using dental model resin (Type II) in a laminar flow hood. The culture bottles were then properly positioned in the ESLCD and connected to the culture medium circulation system. To simulate the in FSU environment, a continuous compressive load was applied to all groups except the pressure group, following our previously published protocols [28]. Based on our previous research findings [29], the traction force parameter was set to 10 kg (100) N), which is considered appropriate for the IVD traction force in animal models. This level of force provides effective biomechanical stimulation without causing tissue damage. The traction force group received an additional 10 kg traction force for 30 minutes daily, in addition to the baseline compression. The culture medium was replaced daily, and the culture environment was maintained at 37°C with 5% CO2 in an incubator. The control group underwent the same medium replacement frequency and environment as the pressure and traction force groups. Samples were collected for analysis on days 0 and 7 of loading.

2.2.4. Histomorphological Analysis

At each time point, motion segments were extracted from each group (n = 4) and fixed overnight in 10% formalin. Decalcification was performed in 19% EDTA for up to 21 days, followed by paraffin embedding. Midsagittal sections were cut at 4 µm intervals and subjected to Hematoxylin and Eosin (H&E) staining and Safranin O-Fast Green staining.

2.2.5. Immunofluorescence Staining

At each time point, motion segments were extracted from each group (n = 4). Standard procedures were employed for deparaffinization and rehydration. Antigen retrieval was performed using EDTA antigen retrieval buffer (pH 9.0) under high-pressure conditions. Immunofluorescence staining was then performed. Images were captured using an inverted fluorescence microscope (Olympus Corporation, Japan) with the following excitation and emission wavelengths: UV excitation 330-380 nm, emission 420 nm; FITC green light excitation 465-495 nm, emission 515-555 nm; CY3 red light excitation 510-560 nm, emission 590 nm. For each fluorescence image, three random equal areas were selected for each indicator. Image-Pro Plus software was used to analyze the images and record the mean optical density for each indicator across different groups. Statistical analysis was subsequently performed on these data.

2.3. Statistical Analysis

Statistical analysis was performed using SPSS software, version 22.0 (IBM Corp., Armonk, NY, USA). Data collected from a minimum of three independent experiments were expressed as mean ± standard deviation (SD). For comparisons between two groups, Student's t-test was utilized, while Analysis of Variance

(ANOVA) was applied for comparisons among multiple groups. A P-value of less than 0.05 was considered statistically significant.

3. RESULTS

3.1. Isolation and Characterization of NPCs-exo

Step 1 CCK-8 analysis revealed comparable NPCs' viability between Blank (standard culture plates) and Control (Flexcell system) groups, confirming the tension system's non-cytotoxic nature. The B-1 group (10% strain, 1 Hz, 24 hours cyclic tension) demonstrated significantly higher viability than Control, Blank, and A-1 groups (p<0.05), establishing these parameters as the screening criteria for Step 2 (Fig. 1A1).

In Step 2 testing, the B-2 group (maintaining 10%/ 1 Hz/ 24 hours parameters) showed enhanced viability versus Control (p<0.05), while A-2 exhibited no significant changes, and Group C displayed markedly reduced viability. This confirmed B-2 parameters as the optimal CMT conditions for subsequent NPCs activation studies (Fig. 1A2).

TEM revealed that NPCs-exo were circular or elliptical in shape with distinct vesicular membranes. Western blot analysis confirmed the expression of exosome marker proteins CD63 and Tsg101, while the negative marker GAPDH was absent, validating the characteristic membrane protein profile of the extracted NPCs-exo. NTA showed that NPCs-exo had an average diameter of 110.1-134.3 nm. consistent with the typical size range of exosomes (Fig. 1B-D).

Flow cytometry analysis using CFSE staining was employed to detect NPCs-exo. CFSE passively diffuses into cells, with CFSE-positive particles representing intact exosomes. The results demonstrated that both the CMT and No-CMT groups contained abundant exosomes compared to the Blank control group (no dve or test substance added). Moreover, the CMT group exhibited a higher concentration of NPCs-exo than the No-CMT group (Fig. 1-E).

3.2. NPCs Uptake of NPCs-exo Enhances Viability and Reduces Apoptosis

Following a 24-hour co-culture period involving PKH67-labeled NPCs-exo and NPCs, confocal laser scanning microscopy analysis revealed an absence of green punctate fluorescence in the Control group. In contrast, both experimental groups displayed green punctate fluorescence, confirming the successful uptake of NPCs-exo by NPCs (Fig. 2A). CCK-8 absorbance assays assessing NPCs proliferation indicated no statistically significant difference between the No-CMT group and the Control group (P > 0.05). Conversely, the CMT group exhibited a marked increase in proliferative activity relative to the Control group (p < 0.01), suggesting that NPCs-exo secreted under CMT conditions significantly enhance NPCs' viability (Fig. 2B).

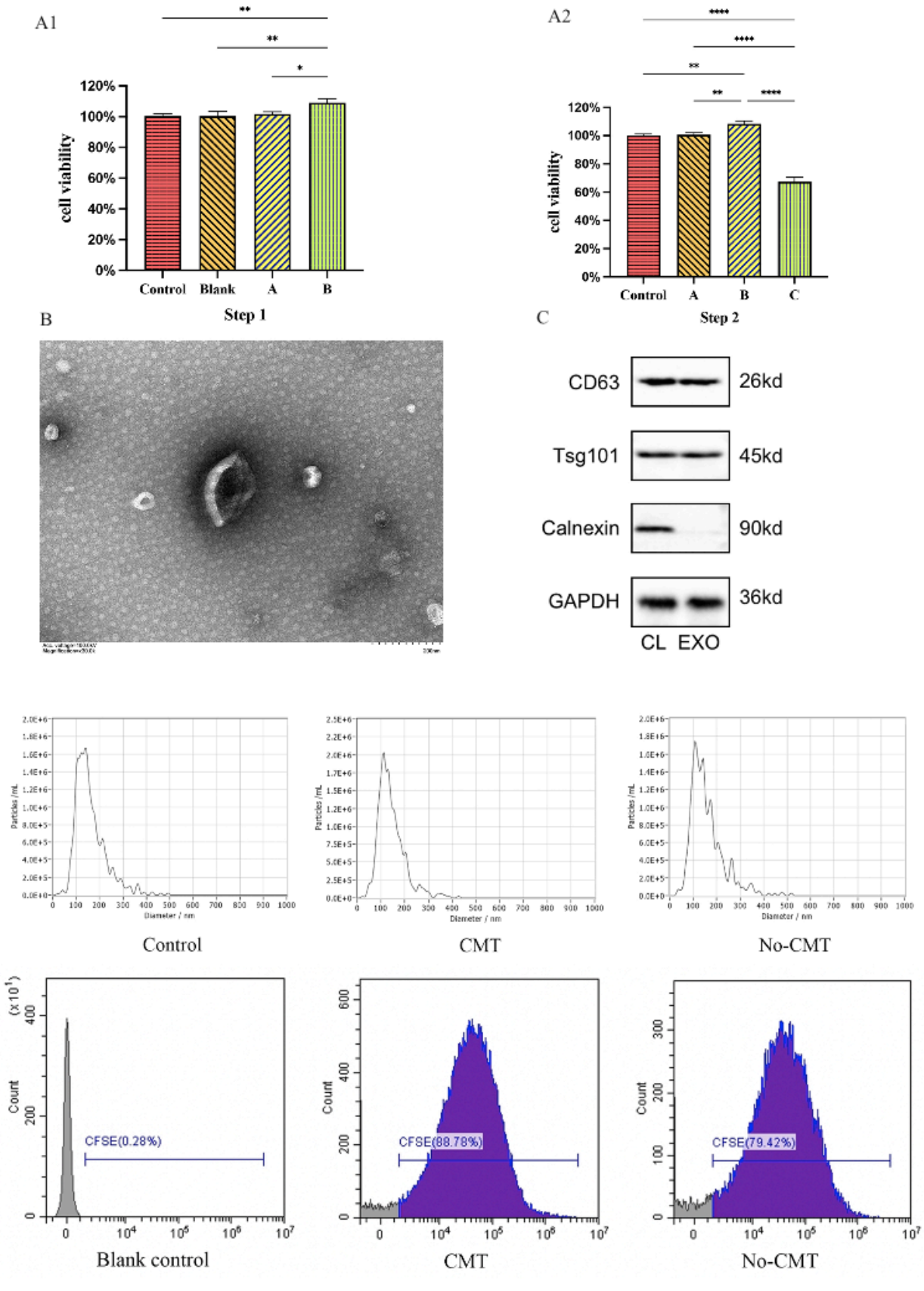


Fig. (1). Optimization of CMT parameters and characterization of NPCs-exo. A1-2: Viability assay of NPCs; B: Transmission electron microscopy images of NPCs-exo (scale bar = 200 nm); C: Western blot analysis of NPCs-exo; D: Nanoparticle tracking analysis of NPCs-exo; E: Concentration measurement of NPCs-exo. (*p < 0.05, **p < 0.01, and ****p < 0.0001). (*A higher resolution / colour version of this figure is available in the electronic copy of the article*).

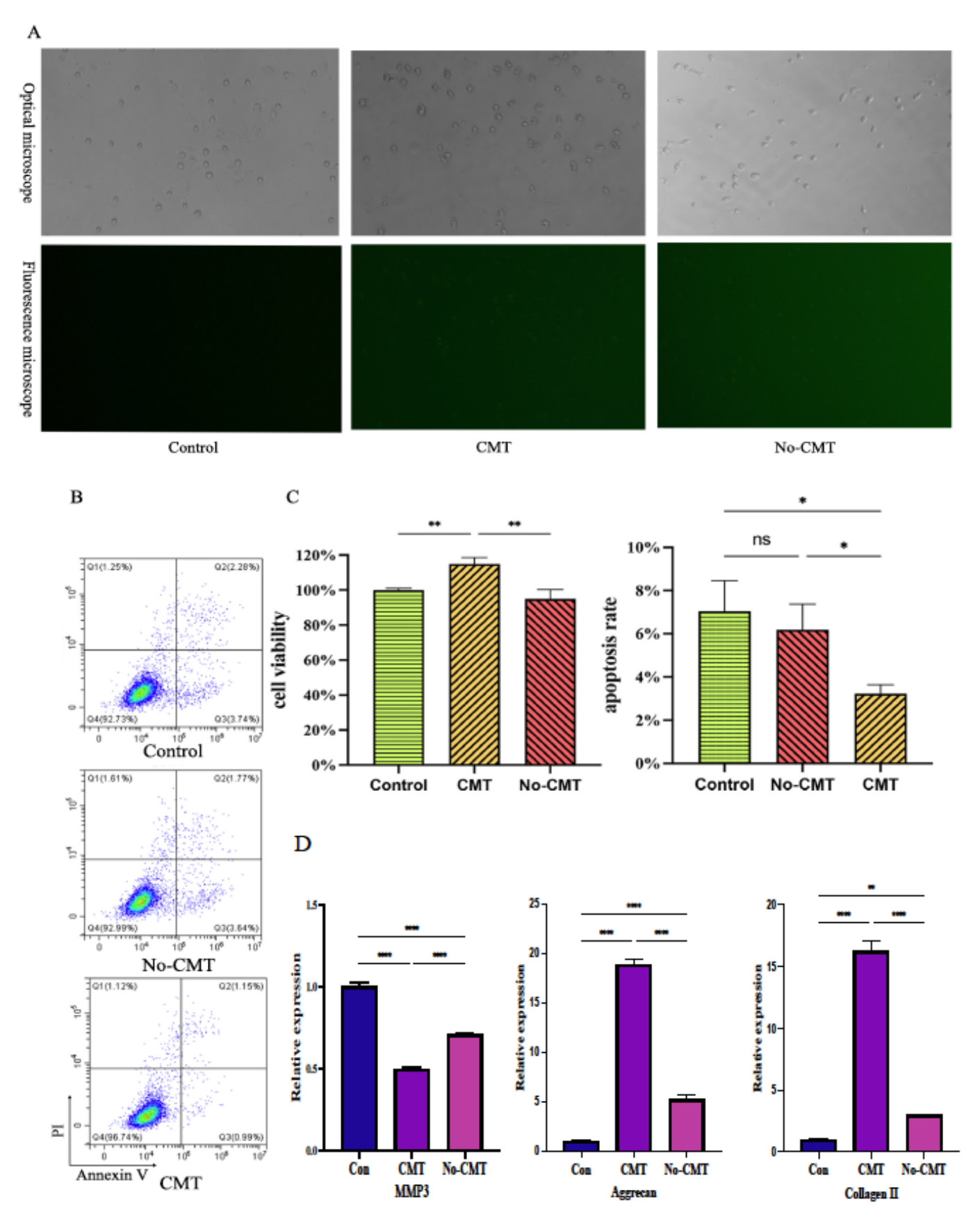
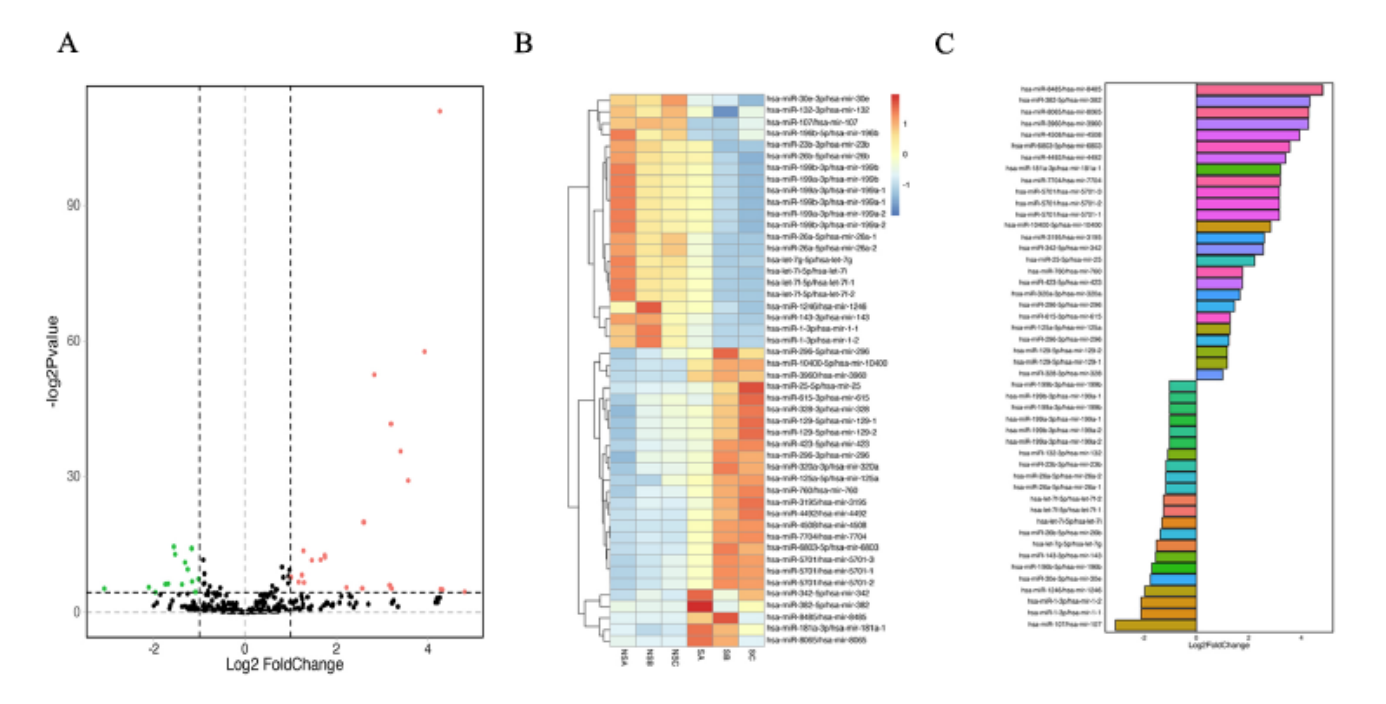


Fig. (2). Analysis of outcomes following the co-culture of NPCs-exo and NPCs. A: Fluorescence microscopy images of NPCs co-cultured with NPCs-exo; B: Flow cytometry analysis of NPCs co-cultured with NPCs-exo; C: Assessment of NPC viability and apoptosis; D: qPCR analysis of MMP3, Aggrecan, and Collagen II expression in NPCs. (*p < 0.05 and **p < 0.01). (A higher resolution / colour version of this figure is available in the electronic copy of the article).



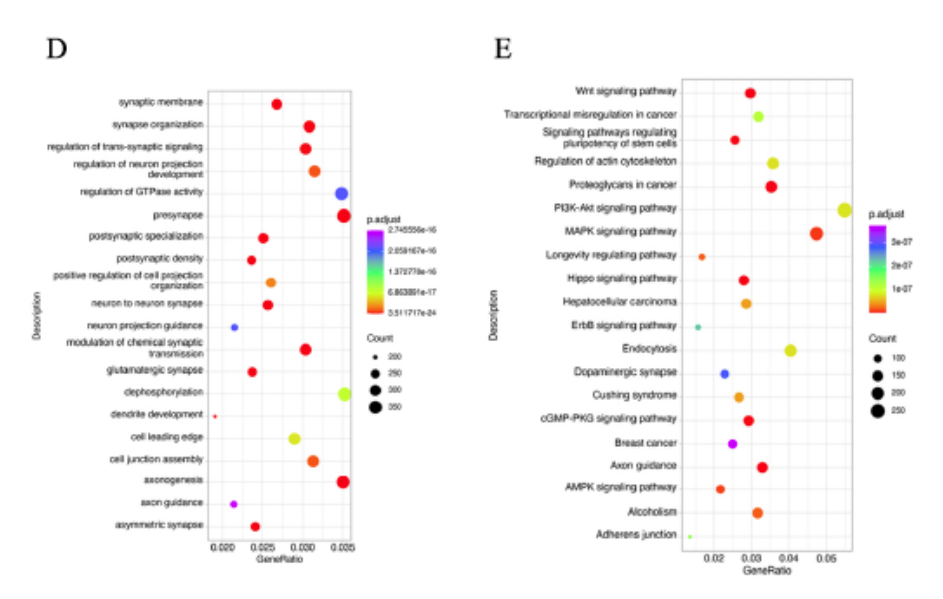


Fig. (3). MiRNA high-throughput sequencing outcomes and differential expression selection and analysis. A-B: Volcano plot and heatmap of high-throughput sequencing of miRNAs in NPCs-exo; C: The top 40 miRNAs with the most significant expression changes in NPCs-exo based on high-throughput sequencing; D-E: GO and KEGG enrichment results of differentially expressed miRNAs between the two groups of NPCs-exo. (*A higher resolution / colour version of this figure is available in the electronic copy of the article*).

Flow cytometry analysis was conducted to assess apoptosis in NPCs. The results from the Annexin V-PI staining assay indicated no statistically significant difference in apoptosis rates between the No-CMT group and the Control group (p > 0.05). In contrast, the CMT group demonstrated a significantly reduced

apoptosis rate compared to the Control group (p < 0.05), suggesting that NPCs-exo secreted under CMT conditions may inhibit apoptosis in NPCs (Fig. **2C**). Furthermore, relative mRNA expression analysis revealed that both the CMT and No-CMT groups exhibited significantly elevated levels of Aggrecan and

Collagen II mRNA compared to the Control group (p < 0.05) (Fig. **2D**). (For qPCR curve, see Supplementary Fig. **1**).

3.3. Regulation of the Wnt/β-catenin Pathway via miR-8485 Targeting GSK-3β

High-throughput sequencing was utilized examine miRNA expression profiles in NPCs-exo. By applying differential expression criteria of llog2 (Foldchange)| > 1 and p < 0.05, a total of 48 differentially expressed miRNAs were identified, comprising 26 upregulated and 22 downregulated miRNAs. Subsequent target gene prediction was conducted for these differentially expressed miRNAs. Enrichment analysis using the KEGG database identified the top 20 pathways, prominently featuring the Wnt signaling pathway, PI3K-Akt signaling pathway, MAPK signaling pathway, and ErbB signaling pathway. Additionally, GO database enrichment analysis underscored functions associated with neuronal and synaptic growth and regulation, trans-synaptic signaling, and mediation and regulation of the cellular environment and movement. To further refine the selection of differentially expressed miRNAs, more stringent criteria were applied: |log2(Foldchange)| > 1 and p < 0.05 for the top 10 upregulated miRNAs. In descending order of log2(Foldchange) values, these were: miR-8485, miR-382-5p, miR-8065, miR-3960, miR-4508, miR-6803-5p, miR-4492, miR-181a-3p, miR-7704, and miR-5701. Consequently, miR-8485, which showed the highest upregulation, was selected for this study (Fig. 3A-E).

Through the use of six target gene prediction databases—TargetScan, miRDB, miRbase, miRTarBase, miRWalk, and miRPathDB-75 intersecting target genes for miR-8485 were identified, including GSK-3\beta. (Supplementary 2). The binding sites between GSK-3\$\beta\$ and miR-8485 were also predicted (Fig. 4A-B). By transfecting miR-8485 mimics, overexpression of miR-8485 was achieved. aPCR was employed to measure the expression levels of miR-8485, GSK-3β, wnt3a, and β-catenin in NPCs, NPCs+NPCs-exo, and NPCs+NPCs-exo+miR-8485 mimics groups. This confirmed that miR-8485 can be transported into NPCs through NPCs-exo and can reduce GSK-3\beta expression while altering the expression of key genes in the Wnt/β-catenin pathway (Fig.

A dual-luciferase reporter assay confirmed the targeting relationship between miR-8485 mimics and GSK-3\(\beta\). Further validation through qPCR and Western blot experiments demonstrated that miR-8485 targets GSK-3β to regulate the Wnt/β-catenin pathway (Fig. 4D-E).

3.4. Evaluation of Tissue Morphology and ECM **Indicators in Animal Models**

Safranin O-Fast Green staining revealed that the control group exhibited intact morphology of the NP and CEP, with orderly cell arrangement and abundant chondrocytes. The pressure group showed cartilage

endplate deformation under abnormal pressure, while the traction group demonstrated notably improved tissue deformation, albeit with some degree of cartilage endplate deformation and chondrocyte loss still present (Fig. **5A-B**).

H&E staining results indicated that the control group maintained an ordered overall structure of the IVD tissue, with abundant NPCs visible in the NP, and an orderly AF structure encasing the NP without rupture. The pressure group, under prolonged abnormal pressure, exhibited AF rupture, NP morphological abnormalities with extrusion, and significant NPCs loss. The traction group exhibited better morphology compared to the pressure group, with relatively ordered AF and NP structures and higher NPCs content, although some NPCs loss was still observed.

Regarding ECM-related indicators Collagen II, Aggrecan, and MMP3, both pressure and traction groups showed significant differences compared to the control group (p < 0.05). The traction group exhibited significant differences in Collagen II and Aggrecan expression compared to the pressure group (p < 0.05) (Fig. **5C-D**).

Table 2. Primer sequences.

Item	Primer sequences	
Collagen II	F: TGGACGCCATGAAGGTTTTCT;	
	R: TGGGAGCCAGATTGTCATCTC	
Aggrecan	F: GCCCAAGACTACCAGTGGAT	
	R: GCGTTTGTAGGTGGTGGCTG	
MMP3	F: CTGGACTCCGACACTCTGGA;	
	R: CAGGAAAGGTTCTGAAGTGACC	
GSK-3β	F: GGCAGCATGAAAGTTAGCAGA;	
	R: GGCGACCAGTTCTCCTGAATC	
Wnt3a	F: TAGGAAGAGAGGTCCAGCCC;	
	R: CTCCAGGAAAGCGGACCATT	
β-catenin	F: AAAGCGGCTGTTAGTCACTGG;	
	R: CGAGTCATTGCATACTGTCCAT	
GAPDH	F: TCATTGACCTCAACTACATGG;	
	R: TCGCTCCTGGAAGATGGTG	
miR-8485	F: TCGGCAGGCACACACACACAC;	
	R: CTCAACTGGTGTCGTGGAGT	

4. DISCUSSION

In this study, CMT was employed to simulate traction forces, and its effects were investigated on NPC-exo secretion at the cellular level. Appropriate mechanical stimulation has been shown to regulate cell growth and differentiation [30]. CMT is a common method of applying mechanical stimulation in cellular studies. The impact of CMT on cells is mainly demonstrated through its regulation of cell proliferation and differentiation [31, 32]. Considering the importance

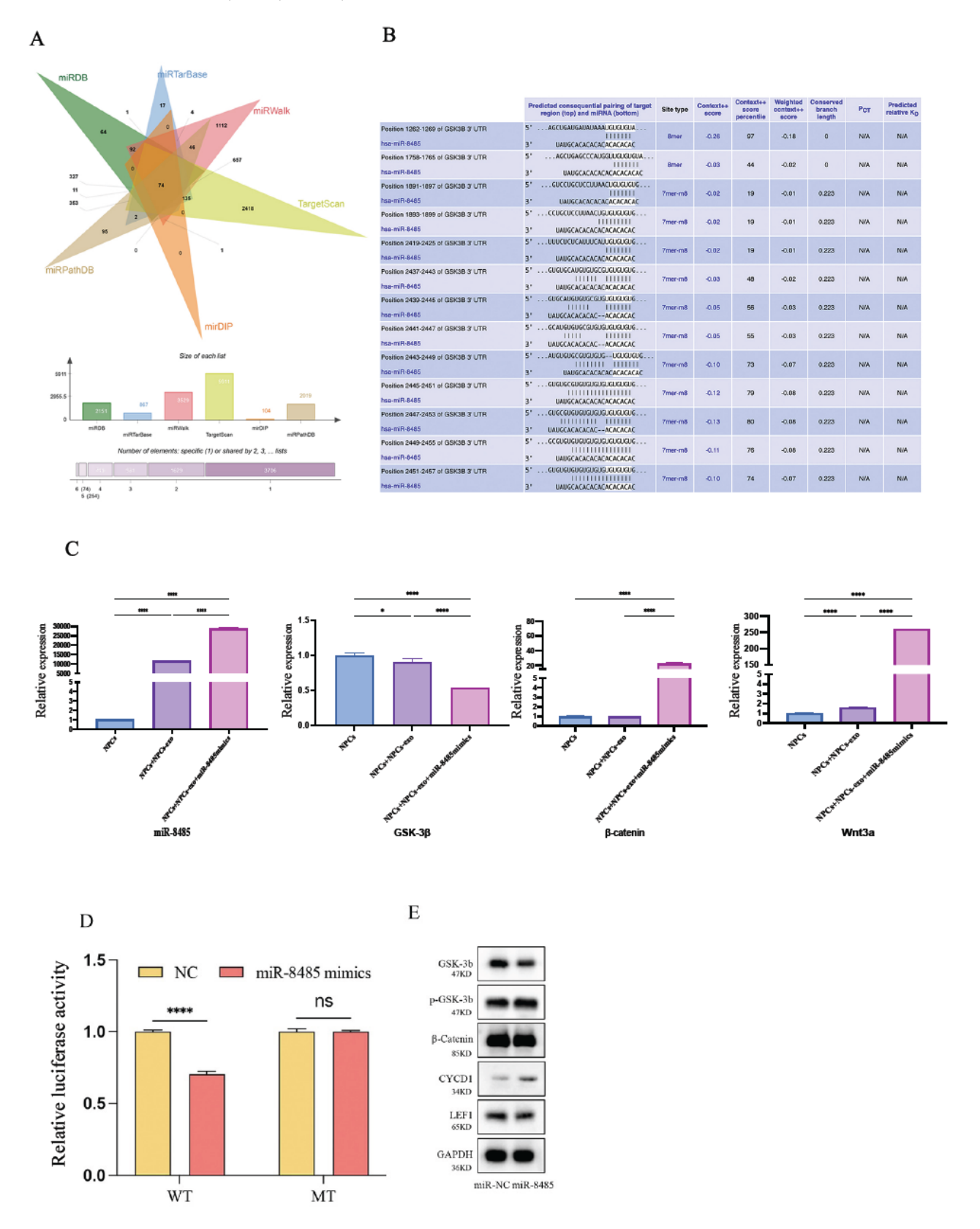


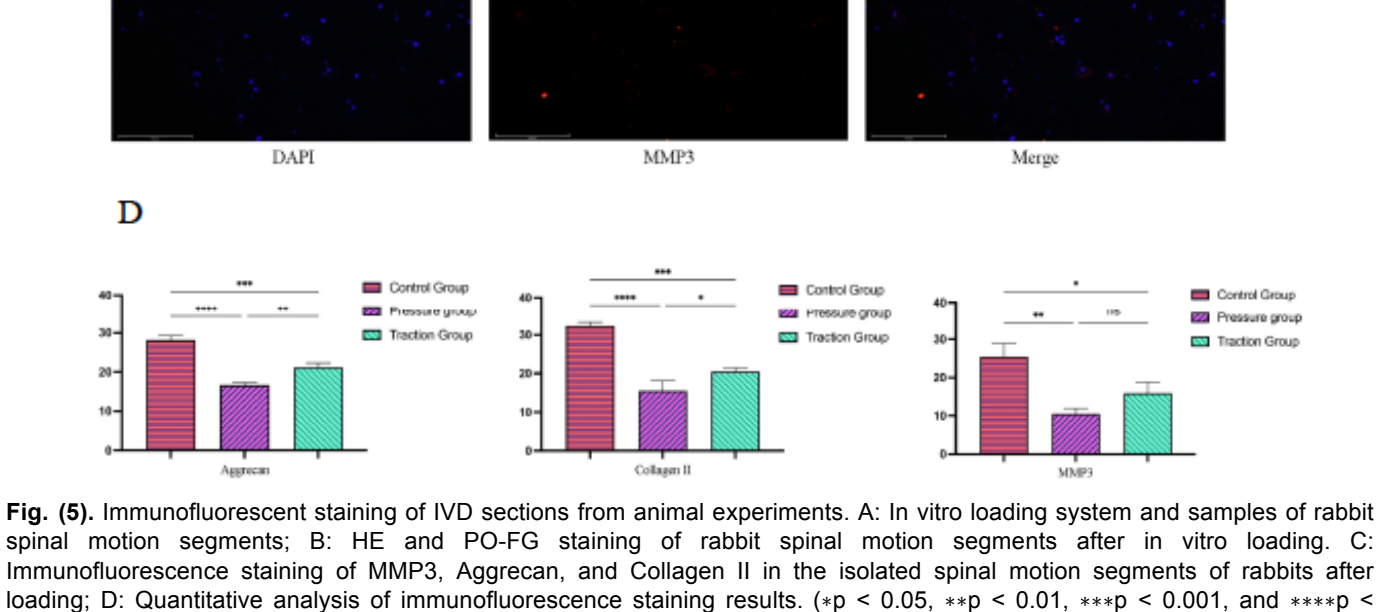
Fig. (4). Analysis of miR-8485 target genes, validation of targeting, and staining in animal experiments. A: Venn diagram illustrating miR-8485 target gene predictions based on six databases identified 74 overlapping genes, including GSK-3β; B: Bioinformatics prediction of the miR-8485 binding site on GSK-3β; C: qPCR analysis of miR-8485, GSK-3β, wnt3a, and β-catenin expression; D: Dual-luciferase assay showing the targeting relationship between miR-8485 and GSK-3β, wt = wild-type; MT = mutant.; E: Western blot analysis of key factors in the Wnt/β-catenin pathway following miR-8485 overexpression transfection; (*p < 0.05 and ****p < 0.0001). (A higher resolution / colour version of this figure is available in the electronic copy of the article).

DAPI

DAPI

Α

В



spinal motion segments; B: HE and PO-FG staining of rabbit spinal motion segments after in vitro loading. C: Immunofluorescence staining of MMP3, Aggrecan, and Collagen II in the isolated spinal motion segments of rabbits after loading; D: Quantitative analysis of immunofluorescence staining results. (*p < 0.05, **p < 0.01, ***p < 0.001, and ****p < 0.0001). (A higher resolution / colour version of this figure is available in the electronic copy of the article).

of CMT in IVDD research, the widely accepted Flexcell tension system, a computer-controlled bioreactor, was employed. These bioreactors apply static and cyclic strain to different cell types cultured as 2D monolayers or embedded in 3D hydrogel models, enabling the evaluation of cellular responses to mechanical strain [33, 34]. This device has been widely used in published research and is applicable to almost all cell types, including chondrocytes, stem cells, and neuronal cells [35-39]. As a result, it ensures stable and sustained CMT loading during NPC culture.

Additionally, CMT can alter the expression of various intracellular miRNAs and participate in the progression of multiple human diseases by regulating the relationship between miRNAs and their target cells [40]. In IVD cell research, a single-cell transcriptomic analysis revealed biomechanical loading induces an imbalance that leads to ossification during NPCs degeneration [41]. CMT has been shown to regulate matrix metabolism, autophagy, and cytoskeletal arrangement in cartilage endplate cells through MAPK and Wnt/β-catenin pathways [42]. Prolonged CMT can induce calcification of cartilage endplate cells and downregulate ankh gene expression [43], while shortterm CMT can increase ankh gene expression in these cells via TGF-β1 and p38 pathways [44]. However, studies applying CMT to NPCs are relatively scarce. Feng et al. [45] demonstrated that under conditions of 20% strain at 1 Hz frequency, NPCs exhibited significant premature senescence following activation of the p53-p21-Rb pathway. CMT at 20% strain can induce endoplasmic reticulum stress and apoptosis in rat annulus fibrosus cells [46]. In summary, CMT has been shown to participate in the regulation of complex biological processes and signaling pathways in IVD.

We examined changes in NPCs' viability, apoptosis, ECM production, and Wnt/β-catenin pathway-related factors through co-culture of NPCs with NPC-exos under CMT conditions. Previous studies have demonstrated that 20% strain can significantly induce apoptosis in NPCs [20, 45]. Therefore, to maximize NPC viability, we screened CMT parameters to avoid excessive apoptosis that might reduce NPC-exo secretion. Results from NPC viability assays following CMT application revealed that parameters of 10% strain, 1 Hz frequency, for 24 hours effectively promoted NPC viability, while higher CMT parameters significantly reduced it. Consequently, we selected these parameters for CMT loading to efficiently isolate NPC-exos. Previous research has similarly shown that mechanical stimulation within certain limits can promote cell proliferation. Wahlsten et al. [47] induced rapid fibroblast proliferation through mechanical stretching, while Yang et al. [48] found that CMT enhanced human periodontal ligament cell proliferation and differentiation through YAP activation.

By co-culturing NPC-exos with NPCs, we demonstrated that NPCs can efficiently take up NPC-exos. First, exosomal transmembrane proteins can directly interact with signaling receptors on target cells [49]. Second, exosomes can fuse with the recipient cell

membrane and deliver their contents into the cytoplasm [50]. Third, exosomes can be internalized by recipient cells through endocytosis, potentially traversing the recipient cell and being released to adjacent cells, or being degraded within the recipient cell [51]. Building on this foundation, we examined NPCs after NPC-exo uptake. The results demonstrated that CMT-induced NPC-exosomes effectively promoted NPC proliferation and inhibited apoptosis. Previous research [52] has shown that exosomes can regulate NPC viability, apoptosis, and ECM synthesis by influencing the Wnt/β-catenin pathway. Therefore, we hypothesized that NPC-exosomes might also affect NPCs by modulating the Wnt/β-catenin pathway. GSK-3β can phosphorylate β-catenin, leading to its degradation and inactivation, thus reducing Wnt/β-catenin pathway activity. GSK-3β can phosphorylate β-catenin, leading to its degradation and inactivation, thus reducing Wnt/β-catenin pathway activity [53-55].

The Wnt/β-catenin pathway plays a crucial role in stem cell renewal, cell proliferation, and differentiation during embryonic development and adult tissue homeostasis [56-58]. In the context of IVD, Wnt signaling plays a crucial role in regulating disc cell function and maintaining matrix homeostasis. Its dysregulation has been linked to heightened catabolic activity, leading to increased ECM degradation and inflammation. In the canonical Wnt/β-catenin pathway, activated β-catenin accumulates in the cytoplasm and translocates to the nucleus, initiating downstream target gene transcription [59]. The Wnt/β-catenin signaling pathway is interconnected with several other known pathways associated with IVD, forming a complex interaction network that influences the pathogenesis of IDD. It interacts with pathways such as Transforming Growth Factor-β (TGF-β) and Bone Morphogenetic Protein (BMP), thereby regulating ECM synthesis and cellular differentiation. Additionally, its crosstalk with the NF-kB signaling pathway modulates cellular senescence and ECM metabolism in disc degeneration [60]. This interaction can regulate the expression of enzymes, such as MMPs, and the degradation of the extracellular matrix, thereby influencing intervertebral disc health, which is consistent with the findings of this study. Moreover, numerous studies have demonstrated that the Wnt/βcatenin signaling pathway can be regulated by exosome-derived miRNAs. MiR-31 carried by bone marrow mesenchymal stem cell-derived exosomes [61] inhibits NFAT5 expression, leading to Wnt/β-catenin pathway activation, thereby promoting NPC proliferation and reducing cell apoptosis and ECM degradation. Conversely, miR-532 downregulates Wnt/β-catenin signaling and induces human nucleus pulposus cell apoptosis by targeting Bcl-9 [62].

NPCs have been shown to be one of the internal factors responsible for IVDD, as they can target MMP-13 and prevent extracellular matrix degradation by delivering EXO miR-27a via autophagy [63]. At the same time, due to their degeneration, exosomes from NPC stem cells in degenerated intervertebral discs exacerbate annulus fibrosus cell degradation via Let-

7b-5p [64]. This study provides evidence of the influence of NPCs-exo on IVDD under mechanical changes. MiR-8485 is a miRNA that has not been extensively studied, but existing research indicates its role in arthritis and cartilage degeneration. MiR-8485 alleviates IL-1β-induced chondrocyte inflammation by suppressing CRLF1 expression [65]. It can regulate the Wnt/β-catenin signalling pathways to facilitate chondrogenesis [66]. Our research also corroborates its role in regulating the Wnt/β-catenin pathways, which are implicated in bone and joint degenerative diseases. This study marks the first instance of its application in conjunction with EXO, demonstrating significant potential for future research into related diseases. Moreover, compared to other miRNAs, miR-8485 exhibits a distinct advantage in its sensitivity to the biomechanics of the IVD. It shows significantly differential expression in EXO under mechanical stress [67]. Given that mechanical factors are an inevitable contributor to the pathogenesis of IVDD and represent a primary physiological function of the disc [68, 69], these characteristic underscores the unique role of miR-8485 in IVDD research. Studies have reported that EXOs secreted by degenerated NPCs can induce macrophage M1 polarization, thereby promoting IVDD [70]. The role of miR-8485 in this process may be a promising area for further investigation.

SU loading is a commonly used technique in ex vivo IVD degeneration models [9, 71]. Previous studies have demonstrated that under sustained compressive loading of the FSU, IVDs initially undergo morphological changes. With prolonged loading, the annulus fibrosus gradually stretches and deforms, the nucleus pulposus shifts from the central region of the IVD, and the expression of collagen type II and aggrecan in IVD tissues decreases [26, 72]. Additionally, vascular budding and VEGFA expression in the cartilage endplate progressively decline [29].

Conservative treatment is the preferred approach for IVDD-related diseases, encompassing methods such as pharmacotherapy, rehabilitation exercises, traction, physiotherapy, and manual manipulation [73-75]. Traction is one of the most used and effective treatments for certain spinal disorders [76-79], with a favorable safety profile [80]. However, the underlying mechanisms of traction therapy remain inadequately elucidated. In this study, we employed an ex vivo combined with cellular experiments demonstrate the potential mechanism by which traction contributes to the attenuation of IVDD. Currently, much research has been carried out on the mechanical pathogenic factors of IVDD, but studies on mechanical treatment factors are limited. We believe that more attention should be given to the basic research on traction therapy for IVDD. To this end, we have developed an ex vivo experimental platform featuring a fully sterile liquid circuit and computer-controlled mechanical and fluidic modulation. This system enables precise regulation of both mechanical and culture environments, allowing for ex vivo spinal tissue cultivation with scientifically managed conditions. Furthermore, it facilitates three-dimensional mechanical loading, including tensile, compressive, and rotational forces [29, 81].

Study Limitations

In this study, an ex vivo rabbit model was utilized, and extensive experiments were conducted to optimize the device for better simulation of the human spinal biomechanical environment. Additionally, we aimed to ensure that the device could withstand both compressive and tensile forces. However, inherent differences between human and rabbit spinal microenvironments, such as variations in nutrient diffusion and vertical loading patterns, remain unavoidable. Furthermore, the research was confined to axial stress, whereas the IVD in humans experiences multi-directional forces. These limitations necessitate further in-depth investigations in future studies.

CONCLUSION

CMT enhances the secretion of NPCs-exo, which are internalized by NPCs, resulting in elevated NPCs activity and reduced apoptosis. Mechanistically, these exosomes deliver miR-8485 to target and modulate GSK-3β, thereby activating the Wnt/β-catenin pathway. This cascade promotes NPCs viability and extracellular synthesis while suppressing matrix apoptosis, ultimately attenuating IVDD progression. Animal experiments validated the in vitro findings, with immunofluorescence staining demonstrating that mechanical traction robustly enhances extracellular matrix expression in the intervertebral disc and stress-induced morphological ameliorates degeneration.

AUTHOR'S CONTRIBUTIONS

The authors confirm their contribution to the paper as follows: conceptualization; JZ, data collection; YD, visualization; RX and HX, analysis and interpretation of the results; GW, writing - original draft preparation; CC, SZ, LZ, KZ, PZ, and WZ, and writing - reviewing and editing; XW. All authors reviewed the results and approved the final version of the manuscript.

LIST OF ABBREVIATIONS

IVDD = Intervertebral disc degeneration

NP Nucleus pulposus

NPCs Nucleus pulposus cells NPCs-exo = NPCs-derived exosomes CEP Cartilaginous endplate **CEPCs** Cartilaginous endplate cells

ETHICS APPROVAL AND CONSENT TO **PARTICIPATE**

This study was approved by the Ethics Committee of China Academy of Chinese Medical Sciences (approval numbers: WJEC-KT-2020-014-P001 and 20180406). The studies involving humans were approved by the Ethics Committee of Wangjing Hospital, China Academy of Chinese Medical Sciences. Following legal and ethical guidelines, we submitted the experimental design protocol, which was approved by the ethics committee under approval number WJEC-KT-2020-014-P001.

HUMAN AND ANIMAL RIGHTS

Research Involving Humans

For the original human samples, NPC samples were obtained from Wangjing Hospital, China Academy of Chinese Medical Sciences. All procedures performed in studies involving human participants were in accordance with the ethical standards of the institutional and/or research committee and with the 1975 Declaration of Helsinki, as revised in 2013..

RESEARCH INVOLVING ANIMALS

All experimental procedures involving animals were conducted in accordance with the standards outlined in the 8th edition of the Guide for the Care and Use of Laboratory Animals. This study adheres to internationally accepted standards for animal research, following the 3Rs principle. The ARRIVE guidelines were employed for reporting experiments involving live animals, promoting ethical research practices.

CONSENT FOR PUBLICATION

The participants provided their written informed consent to participate in this study.

AVAILABILITY OF DATA AND MATERIALS

All the data and supportive information are provided within the article.

FUNDING

National Key Research and Development Program of China (No. 2021YFC1712800); The National Natural Science Foundation of China (No. 82274557, 81930118); Beijing Natural Science Foundation Grant (No. 7242262); National Key Research Development Program of China (No. 2021YFC1712800); The Youth Talent Support Project of the Chinese Association of Traditional Chinese Medicine (No. 2022-QNRC2-B26); Key Collaborative Research Project of the Medical Engineering Interdisciplinary Project of the Science and Technology Innovation Engineering of the Chinese Academy of Traditional Chinese Medicine (No. Cl2023C032YGL); The Chinese Academy of Traditional Chinese Medicine Wangjing Hospital has independently selected a special topic for research (No. 2WJYY-ZZXT-2023-23); Special Program for the Training of Excellent Young Scientific and Technological Talents under the Basic Research Operating Expenses of the China Academy of Chinese Medicine (No. ZZ13-YQ-038) provided funding for this study.

CONFLICT OF INTEREST

The authors declare no conflict of interest, financial or otherwise.

ACKNOWLEDGEMENTS

Declared none.

REFERENCES

- [1] Rodrigues-Pinto R, Richardson SM, Hoyland JA. An understanding of intervertebral disc development, maturation and cell phenotype provides clues to direct cell-based tissue regeneration therapies for disc degeneration. Eur Spine J 2014; 23(9): 1803-14. http://dx.doi.org/10.1007/s00586-014-3305-z PMID:
 - nttp://dx.doi.org/10.1007/s00586-014-3305-z PMID: 24777668
- [2] Isa MIL, Teoh SL, Nor MNH, Mokhtar SA. Discogenic low back pain: Anatomy, pathophysiology and treatments of intervertebral disc degeneration. Int J Mol Sci 2022; 24(1): 208
 - http://dx.doi.org/10.3390/ijms24010208 PMID: 36613651
- [3] Keller TS, Hansson TH, Abram AC, Spengler DM, Panjabi MM. Regional variations in the compressive properties of lumbar vertebral trabeculae. Effects of disc degeneration. Spine 1989; 14(9): 1012-9. http://dx.doi.org/10.1097/00007632-198909000-00016 PMID: 2781407
- [4] Adams MA, Dolan P. Spine biomechanics. J Biomech 2005; 38(10): 1972-83. http://dx.doi.org/10.1016/j.jbiomech.2005.03.028 PMID: 15936025
- [5] Priyadarshani P, Li Y, Yao L. Advances in biological therapy for nucleus pulposus regeneration. Osteoarthritis Cartilage 2016; 24(2): 206-12. http://dx.doi.org/10.1016/j.joca.2015.08.014 PMID: 26342641
- [6] Urban JPG, Smith S, Fairbank JCT. Nutrition of the intervertebral disc. Spine 2004; 29(23): 2700-9. http://dx.doi.org/10.1097/01.brs.0000146499.97948.52 PMID: 15564919
- [7] Hickman TT, Rathan-Kumar S, Peck SH. Development, pathogenesis, and regeneration of the intervertebral disc: Current and future insights spanning traditional to omics methods. Front Cell Dev Biol 2022; 10: 841831. http://dx.doi.org/10.3389/fcell.2022.841831 PMID: 35359439
- [8] Boos N, Weissbach S, Rohrbach H, Weiler C, Spratt KF, Nerlich AG. Classification of age-related changes in lumbar intervertebral discs: 2002 Volvo Award in basic science. Spine 2002; 27(23): 2631-44. http://dx.doi.org/10.1097/00007632-200212010-00002 PMID:
 - nttp://ax.doi.org/10.1097/00007632-200212010-00002 PMID 12461389
- [9] Zhan JW, Wang SQ, Feng MS, et al. Constant compression decreases vascular bud and VEGFA expression in a rabbit vertebral endplate ex vivo culture model. PLoS One 2020; 15(6): e0234747. http://dx.doi.org/10.1371/journal.pone.0234747 PMID:
- [10] Cheng Z, Gan W, Xiang Q, et al. Impaired degradation of PLCG1 by chaperone-mediated autophagy promotes cellular senescence and intervertebral disc degeneration. Autophagy 2025; 21(2): 352-73.

32584845

- http://dx.doi.org/10.1080/15548627.2024.2395797 PMID: 39212196
- [11] Sinkemani A, Wang F, Xie Z, Chen L, Zhang C, Wu X. Nucleus pulposus cell conditioned medium promotes mesenchymal stem cell differentiation into nucleus pulposuslike cells under hypoxic conditions. Stem Cells Int 2020; 2020: 1-24.
- http://dx.doi.org/10.1155/2020/8882549 PMID: 33424982
 [12] Hu Y, Zhang X, Lin MQ, et al. Nanoscale treatment of intervertebral disc degeneration: Mesenchymal stem cell exosome transplantation. Curr Stem Cell Res Ther 2023; 18(2): 163-73.

- http://dx.doi.org/10.2174/1574888X17666220422093103 PMID: 35466881
- [13] Zhan J, Cui Y, Zhang P, et al. Cartilage endplate-targeted engineered exosome releasing and acid neutralizing hydrogel reverses intervertebral disc degeneration. Adv Healthc Mater 2025; 14(2): 2403315. http://dx.doi.org/10.1002/adhm.202403315 PMID: 39555665
- Feng X, Li Y, Su Q, Tan J. Degenerative nucleus pulposus [14] cells derived exosomes promoted cartilage endplate cells apoptosis and aggravated intervertebral disc degeneration. Front Mol Biosci 2022; 9: 835976. http://dx.doi.org/10.3389/fmolb.2022.835976 35359595
- Sun Z, Liu B, Liu ZH, et al. Notochordal-cell-derived [15] exosomes induced by compressive load inhibit angiogenesis via the miR-140-5p/Wnt/β-catenin axis. Mol Ther Nucleic Acids 2020; 22: 1092-106. http://dx.doi.org/10.1016/j.omtn.2020.10.021 PMID: 33294295
- Zhang Q, Shen Y, Zhao S, Jiang Y, Zhou D, Zhang Y. [16] miR-15a promotes nucleus mesenchymal stem cells chondrogenic differentiation by targeting MMP-3. Cell Signal 2021; 86: 110083. http://dx.doi.org/10.1016/j.cellsig.2021.110083 PMID: 34252537
- [17] Chen D, Jiang X. Exosomes-derived miR-125-5p from cartilage endplate stem cells regulates autophagy and ECM metabolism in nucleus pulposus by targeting SUV38H1. Exp Cell Res 2022; 414(1): 113066. http://dx.doi.org/10.1016/j.yexcr.2022.113066 35231441
- Chen D, Jiang X, Zou H. hASCs-derived exosomal miR-155-[18] 5p targeting TGFβR2 promotes autophagy and reduces pyroptosis to alleviate intervertebral disc degeneration. J Orthop Translat 2023; 39: 163-76. http://dx.doi.org/10.1016/j.jot.2023.02.004 PMID: 36950198
- [19] Li W, Xu Y, Chen W. Bone mesenchymal stem cells deliver exogenous IncRNA CAHM via exosomes to regulate macrophage polarization and ameliorate intervertebral disc degeneration. Exp Cell Res 2022; 421(2): 113408. http://dx.doi.org/10.1016/j.yexcr.2022.113408 PMID: 36334792
- Yang M, Feng C, Zhang Y, et al. Autophagy protects nucleus [20] pulposus cells from cyclic mechanical tension-induced apoptosis. Int J Mol Med 2019; 44(2): 750-8. http://dx.doi.org/10.3892/ijmm.2019.4212 PMID: 31173175
- [21] Luo L, Jian X, Sun H, et al. Cartilage endplate stem cells inhibit intervertebral disc degeneration by releasing exosomes to nucleus pulposus cells to activate Akt/autophagy. Stem Cells 2021; 39(4): 467-81. http://dx.doi.org/10.1002/stem.3322 PMID: 33459443
- Zhan JW, Feng MS, Zhu LG, Zhang P, Yu J. Effect of static [22] load on the nucleus pulposus of rabbit intervertebral disc motion segment in an organ culture. BioMed Res Int 2016; 2016: 1-10.
- http://dx.doi.org/10.1155/2016/2481712 PMID: 27872846 [23] Wan ZY, Song F, Sun Z, et al. Aberrantly expressed long noncoding RNAs in human intervertebral disc degeneration: A microarray related study. Arthritis Res Ther 2014; 16(5): http://dx.doi.org/10.1186/s13075-014-0465-5 PMID: 25280944
- Pfirrmann CWA, Metzdorf A, Zanetti M, Hodler J, Boos N. [24] Magnetic resonance classification of lumbar intervertebral disc degeneration. Spine 2001; 26(17): 1873-8. http://dx.doi.org/10.1097/00007632-200109010-00011 PMID:
- [25] Liao Z, Luo R, Li G, et al. Exosomes from mesenchymal stem cells modulate endoplasmic reticulum stress to protect against nucleus pulposus cell death and ameliorate intervertebral disc degeneration in vivo. Theranostics 2019; 9(14): 4084-100. http://dx.doi.org/10.7150/thno.33638 PMID: 31281533
- [26] Zhu LG, Feng MS, Zhan JW, Zhang P, Yu J. Effect of static load on the nucleus pulposus of rabbit intervertebral disc

- motion segment in ex vivo organ culture. Chin Med J 2016; 129(19): 2338-46. http://dx.doi.org/10.4103/0366-6999.190666 27647194
- [27] Wang H, Chen X, Hong-Guang X, Ding G, Liu P, Huang D. Correlation between VEGF and HIF-1a expression in vertebral cartilage endplate of cervical spondylosis patients. J Pract Med 2008; 1-9.
- Yin X. The mechanism of BSHXR on nucleus pulposus cells [28] of IDD by regulating Wnt/beta-catenin pathway. Beijing, China: Chinese Academy of Traditional Chinese Medicine 2019; pp. 1-8.
- [29] Zhan JW, Wang SQ, Feng MS, et al. Effects of axial compression and distraction on vascular bud and VEGFA expression in the vertebral endplate of an ex vivo rabbit spinal motion segment culture model. Spine 2021; 46(7):
 - http://dx.doi.org/10.1097/BRS.000000000003816 PMID: 33186278
- Tringides CM, Boulingre M, Khalil A, Lungjangwa T, Jaenisch [30] R, Mooney DJ. Tunable conductive hydrogel scaffolds for neural cell differentiation. Adv Healthc Mater 2023; 12(7): http://dx.doi.org/10.1002/adhm.202202221 PMID: 36495560
- [31] Motie P, Mohaghegh S, Kouhestani F, Motamedian SR. Effect of mechanical forces on the behavior of osteoblasts: A systematic review of in vitro studies. Dent Med Probl 2023; 60(4): 673-86. http://dx.doi.org/10.17219/dmp/151639 PMID: 38133991
- [32] Shen T, Qiu L, Chang H, et al. Cyclic tension promotes osteogenic differentiation in human periodontal ligament stem cells. Int J Clin Exp Pathol 2014; 7(11): 7872-80. PMID: 25550827
- [33] Colombo A, Cahill PA, Lally C. An analysis of the strain field in biaxial Flexcell membranes for different waveforms and frequencies. Proc Inst Mech Eng H 2008; 222(8): 1235-45. http://dx.doi.org/10.1243/09544119JEIM428 19143417
- López-Martínez C, Huidobro C, Albaiceta GM, López-Alonso [34] I. Mechanical stretch modulates cell migration in the lungs. Ann Transl Med 2018; 6(2): 28.
- http://dx.doi.org/10.21037/atm.2017.12.08 PMID: 29430445 Hilscher MB, Sehrawat T, Arab JP, et al. Mechanical stretch [35] increases expression of cxcl1 in liver sinusoidal endothelial cells to recruit neutrophils, generate sinusoidal microthombi, and promote portal hypertension. Gastroenterology 2019; 157(1): 193-209.e9.
 - http://dx.doi.org/10.1053/j.gastro.2019.03.013 PMID: 30872106
- Zhou X, Cao H, Liao T, et al. Mechanosensitive IncRNA H19 [36] promotes chondrocyte autophagy, but not pyroptosis, by osteoarthritis. miR-148a in post-traumatic Noncoding RNA Res 2025; 10: 163-76. http://dx.doi.org/10.1016/j.ncrna.2024.07.005 PMID: 39399379
- Liu C, Gao X, Lou J, et al. Aberrant mechanical loading induces annulus fibrosus cells apoptosis in intervertebral disc degeneration via mechanosensitive ion channel Piezo1. Arthritis Res Ther 2023; 25(1): 117. http://dx.doi.org/10.1186/s13075-023-03093-9 PMID: 37420255
- Liu J, Liu R, Wang H, Zhang Z, Wang J, Wei F. [38] CircPRKD3/miR-6783-3p responds to mechanical force to facilitate the osteogenesis of stretched periodontal ligament stem cells. J Orthop Surg Res 2024; 19(1): 257. http://dx.doi.org/10.1186/s13018-024-04727-7 PMID:
- [39] Hochreiter B, Lindner C, Postl M, et al. Characterizing SV40hTERT immortalized human lung microvascular endothelial cells as model system for mechanical stretch-induced lung injury. Int J Mol Sci 2025; 26(2): 683. http://dx.doi.org/10.3390/ijms26020683 PMID: 39859396
- Feng C, Liu M, Fan X, Yang M, Liu H, Zhou Y. Intermittent [40] cyclic mechanical tension altered the microRNA expression

- profile of human cartilage endplate chondrocytes. Mol Med Rep 2018; 17(4): 5238-46. http://dx.doi.org/10.3892/mmr.2018.8517 PMID: 29393457
- [41] Zhang P, Wang Y, Bai J, et al. Single-cell transcriptomic analysis reveals biomechanical loading-induced imbalance in bone and fat, leading to ossification in lumbar intervertebral disc nucleus pulposus degeneration. J Cell Physiol 2025; 240(1): e31506.

http://dx.doi.org/10.1002/jcp.31506 PMID: 39854079

- [42] Xu H, Zheng Q, Song J, et al. Intermittent cyclic mechanical tension promotes endplate cartilage degeneration via canonical Wnt signaling pathway and E-cadherin/β-catenin complex cross-talk. Osteoarthritis Cartilage 2016; 24(1): 158-68.
- http://dx.doi.org/10.1016/j.joca.2015.07.019 PMID: 26247612

 Xu H, Zhang X, Wang H, *et al.* Intermittent cyclic mechanical tension-induced calcification and downregulation of ankh gene expression of end plate chondrocytes. Spine 2012; 37(14): 1192-7.

 http://dx.doi.org/10.1097/BRS.0b013e318244d989 PMID: 22695244
- [44] Xu H, Zhang X, Wang H, Zhang Y, Shi Y, Zhang X. Continuous cyclic mechanical tension increases ank expression in endplate chondrocytes through the TGF-β1 and p38 pathway. Eur J Histochem 2013; 57(3): 28. http://dx.doi.org/10.4081/ejh.2013.e28 PMID: 24085277
- [45] Feng C, Yang M, Zhang Y, et al. Cyclic mechanical tension reinforces DNA damage and activates the p53-p21-Rb pathway to induce premature senescence of nucleus pulposus cells. Int J Mol Med 2018; 41(6): 3316-26. http://dx.doi.org/10.3892/ijmm.2018.3522 PMID: 29512682
- [46] Zhang YH, Zhao CQ, Jiang LS, Dai LY. Cyclic stretch-induced apoptosis in rat annulus fibrosus cells is mediated in part by endoplasmic reticulum stress through nitric oxide production. Eur Spine J 2011; 20(8): 1233-43. http://dx.doi.org/10.1007/s00586-011-1718-5 PMID: 21336971
- [47] Wahlsten A, Rütsche D, Nanni M, et al. Mechanical stimulation induces rapid fibroblast proliferation and accelerates the early maturation of human skin substitutes. Biomaterials 2021; 273: 120779. http://dx.doi.org/10.1016/j.biomaterials.2021.120779 PMID: 33932701
- [48] Yang Y, Wang BK, Chang ML, Wan ZQ, Han GL. Cyclic stretch enhances osteogenic differentiation of human periodontal ligament cells via YAP activation. BioMed Res Int 2018; 2018: 1-12. http://dx.doi.org/10.1155/2018/2174824 PMID: 30519570
- [49] Munich S, Sobo-Vujanovic A, Buchser WJ, Beer-Stolz D, Vujanovic NL. Dendritic cell exosomes directly kill tumor cells and activate natural killer cells via TNF superfamily ligands. Oncolmmunology 2012; 1(7): 1074-83. http://dx.doi.org/10.4161/onci.20897 PMID: 23170255
- [50] Mulcahy LA, Pink RC, Carter DRF. Routes and mechanisms of extracellular vesicle uptake. J Extracell Vesicles 2014; 3(1): 24641. http://dx.doi.org/10.3402/jev.v3.24641 PMID: 25143819
- [51] Tian T, Zhu YL, Hu FH, Wang YY, Huang NP, Xiao ZD. Dynamics of exosome internalization and trafficking. J Cell Physiol 2013; 228(7): 1487-95. http://dx.doi.org/10.1002/jcp.24304 PMID: 23254476
- [52] Wang H, Li F, Ban W, Zhang J, Zhang G. Human bone marrow mesenchymal stromal cell-derived extracellular vesicles promote proliferation of degenerated nucleus pulposus cells and the synthesis of extracellular matrix through the sox4/wnt/β-catenin axis. Front Physiol 2021; 12: 723220.
 - http://dx.doi.org/10.3389/fphys.2021.723220 PMID: 34777000
- [53] Huang J, Guo X, Li W, Zhang H. Activation of Wnt/β-catenin signalling via GSK3 inhibitors direct differentiation of human adipose stem cells into functional hepatocytes. Sci Rep 2017; 7(1): 40716. http://dx.doi.org/10.1038/srep40716 PMID: 28094799

- [54] Cheng X, Wu C, Xu H, Zou R, Li T, Ye S. miR-557 inhibits hepatocellular carcinoma progression through Wnt/β-catenin signaling pathway by targeting RAB10. Aging 2024; 16(4): 3716-33. http://dx.doi.org/10.18632/aging.205554 PMID: 38364252
- [55] Yang F, Xiong H, Duan L, Li Q, Li X, Zhou Y. MiR-1246 promotes metastasis and invasion of a549 cells by targeting GSK-3B–Mediated WNT/β-catenin pathway. Cancer Res Treat 2019; 51(4): 1420-9. http://dx.doi.org/10.4143/crt.2018.638 PMID: 30913872
- [56] Liu J, Xiao Q, Xiao J, et al. Wnt/β-catenin signalling: Function, biological mechanisms, and therapeutic opportunities. Signal Transduct Target Ther 2022; 7(1): 3. http://dx.doi.org/10.1038/s41392-021-00762-6 PMID:
- [57] Hu L, Chen W, Qian A, Li YP. Wnt/β-catenin signaling components and mechanisms in bone formation, homeostasis, and disease. Bone Res 2024; 12(1): 39. http://dx.doi.org/10.1038/s41413-024-00342-8 PMID: 38987555
- [58] Silwal P, Nguyen-Thai AM, Mohammad HA, et al. Cellular senescence in intervertebral disc aging and degeneration: Molecular mechanisms and potential therapeutic opportunities. Biomolecules 2023; 13(4): 686. http://dx.doi.org/10.3390/biom13040686 PMID: 37189433
- [59] Zhao H, Ming T, Tang S, et al. Wnt signaling in colorectal cancer: Pathogenic role and therapeutic target. Mol Cancer 2022; 21(1): 144. http://dx.doi.org/10.1186/s12943-022-01616-7 PMID: 35836256
- [60] Zhu D, Chen S, Sheng P, Wang Z, Li Y, Kang X. POSTN promotes nucleus pulposus cell senescence and extracellular matrix metabolism *via* activing Wnt/β-catenin and NF-κB signal pathway in intervertebral disc degeneration. Cell Signal 2024; 121: 111277. http://dx.doi.org/10.1016/j.cellsig.2024.111277 PMID: 38944256
- [61] Wang B, Xu N, Cao L, et al. miR-31 from Mesenchymal Stem Cell-Derived Extracellular Vesicles Alleviates Intervertebral Disc Degeneration by Inhibiting NFAT5 and Upregulating the Wnt/β-Catenin Pathway. Stem Cells Int 2022; 2022: 1-16. http://dx.doi.org/10.1155/2022/2164057 PMID: 36311041
- [62] Sun Z, Jian Y, Fu H, Li B. MiR-532 downregulation of the Wnt/β-catenin signaling via targeting Bcl-9 and induced human intervertebral disc nucleus pulposus cells apoptosis. J Pharmacol Sci 2018; 138(4): 263-70. http://dx.doi.org/10.1016/j.jphs.2018.10.007 PMID: 30472057
- [63] Zhang QC, Hu SQ, Hu AN, Zhang TW, Jiang LB, Li XL. Autophagy-activated nucleus pulposus cells deliver exosomal miR-27a to prevent extracellular matrix degradation by targeting MMP-13. J Orthop Res 2021; 39(9): 1921-32. http://dx.doi.org/10.1002/jor.24880 PMID: 33038032
- [64] Zhuang Y, Song S, Xiao D, et al. Exosomes secreted by nucleus pulposus stem cells derived from degenerative intervertebral disc exacerbate annulus fibrosus cell degradation via let-7b-5p. Front Mol Biosci 2022; 8: 766115. http://dx.doi.org/10.3389/fmolb.2021.766115 PMID:
- [65] Yang G, Ji B, Li H, et al. Inhibition of CRLF1 expression by miR-8485 alleviates IL-1β-induced chondrocyte inflammation, apoptosis, and extracellular matrix degradation. Int Immunopharmacol 2025; 144: 113643. http://dx.doi.org/10.1016/j.intimp.2024.113643 PMID: 39580860

35111808

- [66] Li Z, Wang Y, Xiang S, et al. Chondrocytes-derived exosomal miR-8485 regulated the Wnt/β-catenin pathways to promote chondrogenic differentiation of BMSCs. Biochem Biophys Res Commun 2020; 523(2): 506-13. http://dx.doi.org/10.1016/j.bbrc.2019.12.065 PMID: 31898972
- [67] Chang M, Chen Q, Wang B, Zhang Z, Han G. Exosomes from tension force-applied periodontal ligament cells promote mesenchymal stem cell recruitment by altering microRNA profiles. Int J Stem Cells 2023; 16(2): 202-14. http://dx.doi.org/10.15283/ijsc21170 PMID: 36823975

- [68] Chen X, Li Z, Zheng C, Wu J, Hai Y. Expression of MMP1, MMP3, and TIMP1 in intervertebral discs under simulated overload and microgravity conditions. J Orthop Surg Res 2025; 20(1): 71. http://dx.doi.org/10.1186/s13018-025-05508-6 PMID: 39833904
- [69] Feki F, Taktak R, Haddar N, Moulart M, Zaïri F, Zaïri F. Overloading effect on the osmo-viscoelastic and recovery behavior of the intervertebral disc. Proc Inst Mech Eng H 2024; 238(4): 430-7. http://dx.doi.org/10.1177/09544119241232286 PMID:

38480472

- [70] Zhao X, Sun Z, Xu B, et al. Degenerated nucleus pulposus cells derived exosome carrying miR-27a-3p aggravates intervertebral disc degeneration by inducing M1 polarization of macrophages. J Nanobiotechnology 2023; 21(1): 317. http://dx.doi.org/10.1186/s12951-023-02075-y PMID: 37667246
- [71] An HS, Masuda K. Relevance of in vitro and in vivo models for intervertebral disc degeneration. J Bone Joint Surg Am 2006; 88: 88-94.(Suppl. 2) PMID: 16595451
- [72] Liu Q, Liang XF, Wang AG, et al. Failure mechanical properties of lumbar intervertebral disc under high loading rate. J Orthop Surg Res 2024; 19(1): 15. http://dx.doi.org/10.1186/s13018-023-04424-x PMID: 38167031
- [73] Zhang W, Wang G, Xie R, et al. Traditional Chinese exercises on pain and disability in middle-aged and elderly patients with lumbar disc herniation: A systematic review and meta-analysis of randomized controlled trials. Front Med 2023; 10: 1265040. http://dx.doi.org/10.3389/fmed.2023.1265040 PMID: 38020108
- [74] Samanta A, Lufkin T, Kraus P. Intervertebral disc degeneration—current therapeutic options and challenges. Front Public Health 2023; 11: 1156749. http://dx.doi.org/10.3389/fpubh.2023.1156749 PMID: 37483952

- [75] Yang S, Zhang Y, Peng Q, et al. Regulating pyroptosis by mesenchymal stem cells and extracellular vesicles: A promising strategy to alleviate intervertebral disc degeneration. Biomed Pharmacother 2024; 170: 116001. http://dx.doi.org/10.1016/j.biopha.2023.116001 PMID: 38128182
- [76] Vanti C, Panizzolo A, Turone L, et al. Effectiveness of mechanical traction for lumbar radiculopathy: A systematic review and meta-analysis. Phys Ther 2021; 101(3): pzaa231. http://dx.doi.org/10.1093/ptj/pzaa231 PMID: 33382419
- [77] Feng T, Wang X, Bu H, et al. Cervical rotation-traction manipulation for cervical radiculopathy: A systematic review and meta-analysis of randomized control trials. J Pain Res 2024; 17: 4055-70. http://dx.doi.org/10.2147/JPR.S481803 PMID: 39629140
- [78] Cheng YH, Hsu CY, Lin YN. The effect of mechanical traction on low back pain in patients with herniated intervertebral disks: A systemic review and meta-analysis. Clin Rehabil 2020; 34(1): 13-22. http://dx.doi.org/10.1177/0269215519872528 PMID: 31456418
- [79] Jellad A, Kalai A, Chaabeni A, et al. Effect of cervical traction on cervicogenic headache in patients with cervical radiculopathy: A preliminary randomized controlled trial. BMC Musculoskelet Disord 2024; 25(1): 842. http://dx.doi.org/10.1186/s12891-024-07930-z PMID: 39448969
- [80] Tadano S, Tanabe H, Arai S, Fujino K, Doi T, Akai M. Lumbar mechanical traction: A biomechanical assessment of change at the lumbar spine. BMC Musculoskelet Disord 2019; 20(1): 155. http://dx.doi.org/10.1186/s12891-019-2545-9 PMID: 30961554
- [81] Han T, Luo P, Cai C, et al. The influence of different stress loading on the biomechanics of motion segments in isolated rabbit spines. J Biomech 2025; 182: 112592. http://dx.doi.org/10.1016/j.jbiomech.2025.112592 PMID: 39987886